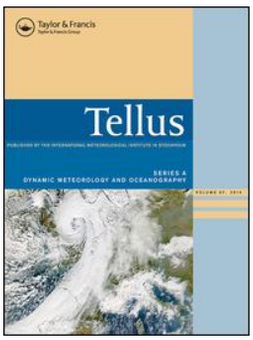

Tellus A: Dynamic Meteorology and Oceanography

ISSN: (Print) 1600-0870 (Online) Journal homepage: https://www.tandfonline.com/loi/zela20

Sensitivity of Southern Ocean sea-ice simulations to different atmospheric forcing algorithms

Achim StÖSsel

To cite this article: Achim StÖSsel (1992) Sensitivity of Southern Ocean sea-ice simulations to different atmospheric forcing algorithms, Tellus A: Dynamic Meteorology and Oceanography, 44:5, 395-413, DOI: 10.3402/tellusa.v44i5.14970

To link to this article: https://doi.org/10.3402/tellusa.v44i5.14970

Tellus (1992), *44A*, 395–413

Sensitivity of Southern Ocean sea-ice simulations to different atmospheric forcing algorithms

By ACHIM STÖSSEL, *Max-Planck-Institut für Meteorologie, Bundesstrasse 55, 2000 Hamburg 13, Germany*

(Manuscript received 4 July 1991; in final form 22 June 1992)

ABSTRACT

Sea ice is sensitively dependent on the fluxes of energy, mass and momentum between the ocean and the atmosphere, making it worth investigating the modification of these fluxes by the respective boundary layers. Complementary to earlier investigations with a coupled sea-ice–oceanic mixed-layer model for the Southern Ocean, the atmospheric forcing in the present investigation is changed from monthly, observational data to daily, essentially modelled values computed by an operational numerical weather-prediction model. Applying these computations directly as atmospheric surface forcing to the sea-ice–oceanic mixed-layer model yields (in first order) encouraging results, indicating the general reliability of these data. As a supplement to the oceanic mixed-layer model, the fluxes derived from the atmospheric forcing are modified in a first step to include the stability dependency of the atmospheric surface-layer. Compared to the application of usual adjustment practices, this leads to improved results, especially with respect to the ice velocities in divergent ice fields. In the next step, the atmospheric forcing level is raised to the geostrophic level thus incorporating the entire atmospheric boundary layer. While the forcing fields become less dependent on the prescribed boundary conditions of the weather-prediction model, the simulations appear to be reasonable only when the near-surface wind forcing is applied, the overall roughness length is increased and the large-scale stability is reduced. This leads to important implications for coupled atmosphere–sea-ice–ocean models.

1. Introduction

Sea ice is an important component in the global climate system and thus subject to various modelling efforts. Dynamic-thermodynamic modelling of Antarctic sea ice was the issue of several authors since 1979. Parkinson and Washington (1979) modelled the sea ice around the entire continent with highly sophisticated thermodynamics but rather crude dynamics. Hibler and Ackley (1983), describing the Weddell Sea region, employed rheological considerations for the dynamics while restricting the thermodynamics. The latter model was extended to include a prognostic oceanic mixed layer [OML] by Lemke et al. (1990), a prognostic snow layer by Owens and Lemke (1990) and, independently, a diagnostic atmospheric boundary layer [ABL] by Koch (1988). With the first two extensions, this model was finally enlarged to simulate the entire Southern Ocean ice pack by Stössel et al. (1990) (in the following referred to as SLO).

Simultaneously, sea ice [SI] was implemented in oceanic general circulation [OGC] models in a variety of ways (van Ypersele, 1986, Maier-Reimer et al., 1991, Manabe et al., 1990, Foreman et al., 1988), the most sophisticated formulation provided by Oberhuber (1990).

A crucial point concerning sea-ice simulations is the strong dependency of the results on the specified forcing fields. The sensitivity to the oceanic forcing in terms of vertical oceanic heat flux was reduced by the employment of an interactive OML model (Lemke et al., 1990). A reduction of the sensitivity with respect to the atmospheric forcing is the main issue of the present paper.

Generally, the atmospheric forcing for dynamic-thermodynamic sea-ice models consists of monthly values from climatologies, which are supposed to be representative for the atmospheric layer

close to the surface. The actual forcing terms are represented by the radiative and turbulent heat fluxes as well as the momentum flux, the last two fluxes usually being calculated by bulk formulas with constant transfer or drag coefficients, respectively. Altogether, this leads to two problems with regard to the atmospheric forcing: the reliability of the data and their translation to surface fluxes.

Concerning the first problem, a physically more consistent representation of the atmospheric variables is believed to be given by analyses from operational numerical weather-prediction [NWP] centers, consisting of a blend of instantaneous observations and model results of the previous forecast run, thus providing spatial and temporal consistency with the general circulation.

With respect to the second problem, alternatively to the widely spread practices of model adjustment to changed boundary conditions (forcing fields), it appears to be more convenient to modify the strength of the forcing by taking into account the local (sub-grid scale) physics in the vicinity of the boundaries. In the present work this is done by considering boundary-layer physics responding to the instantaneous sea-ice conditions provided by the SI model.

Accordingly, the paper constitutes of a hierarchy of boundary-layer modifications of the atmospheric forcing. After illustrating the SI-OML model and describing the forcing data, the impact of model adjustments to direct surface forcing is demonstrated. Next, the atmospheric forcing of the SI-OML model is modified by an atmospheric surface-layer [ASL] parameterisation. Finally, the SI-OML model is coupled to an ABL model including the Ekman layer, the thermal forcing being provided at the geostrophic level. The latter simulations are organised in a series of sensitivity studies. The description of the experiments finishes with an overall discussion, where the various results are analysed and intercompared. At the end, conclusions are given together with implications for further coupling studies.

2. Basic model

The SI-OML model used in this study is identical to the one used in SLO. A detailed description of the model is given in Lemke et al. (1990) and Owens and Lemke (1990). An illustration of the variables involved in the SI-OML model is shown in Fig. 1. They are distinguished between prognostically and diagnostically computed ones, and those which are externally specified (forcing variables).

The shaded parcels floating at the surface ($z = 0$) are supposed to represent sea ice, being characterised by the ice thickness (h_i). The ice is allowed to be snow covered (dotted areas), leading to a variable snow thickness (h_{sn}). Together with the ice compactness (N_i) (i.e., the ice coverage or ice concentration), these variables are prognostically calculated by continuity equations being composed of dynamic and thermodynamic terms. The ice velocity $\boldsymbol{V}_i$ is calculated via a momentum equation with an additional force term due to internal ice stress, employing a viscous-plastic ice rheology (Hibler, 1979). Thus, ridging and rafting effects are implicitly included.

Additional prognostic variables arise from the OML model (Lemke, 1987): the mixed-layer depth h_{o1} (if determined by the entrainment rate), temperature (T_{o1}) and salinity (S_1) of the mixed layer, and the e-folding thicknesses of the thermocline (h_{Tc}) and halocline (h_{Hc}). With the introduction of these scale depths, the mixed-layer variables are not directly dependent on the variables of the second oceanic layer, but rather on mean variables within the pycnocline. The temperature and salinity profiles indicated by full lines are supposed to represent winter situations with a deep mixed layer, being colder and slightly less saline than the layer below, thus representing a marginally stable stratification (Martinson, 1990). In summer (dashed profiles), h_{o1} is shallower, $T_{o1} > T_{o2}$ and S_1 is less than in winter (due to ice melt), which, together with the warming of the mixed layer, generally leads to a stable stratification with h_{o1} being diagnostically determined by the Monin-Obukhov length.

The vertical oceanic (entrainment) heat flux (Q_o) is diagnostically calculated from the mixed-layer variables. Together with the conductive heat flux through the ice (Q_c) it determines the thermodynamic change of ice thickness. The turbulent (Q_{1a}, Q_{se}) and radiative (Q_{1w}, Q_{sw}) heat fluxes combine to the heat balance equation, which is separately calculated over the ice free and the ice covered part of a grid cell, and in the latter case is supplemented by Q_c. Two variables directly

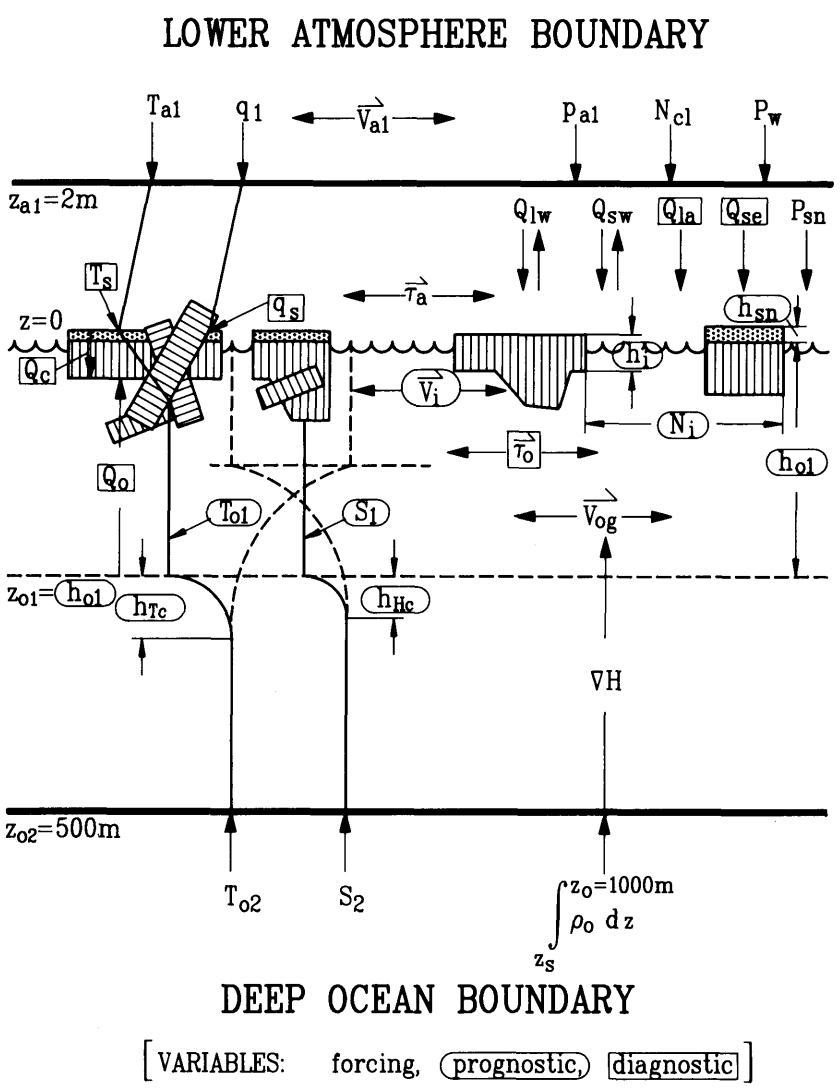

Fig. 1. Viewgraph of the variables of the SI-OML model.

influencing the strength of the atmospheric forcing are the surface temperature (of ice or snow: T_s, being iteratively derived from the heat balance equation; or of the mixed layer: T_{o1}) and the specific humidity at the surface.

The air/ice stress (τ_a) is directly determined by the winds and optionally modified by boundary-layer considerations. The ice/ocean stress (τ_o), on the other hand, is aside from the ocean current, essentially determined by the ice drift.

Finally, forcing variables are specified from the lower atmosphere ($z_{a1} = 2$ m or 10 m) in terms of temperature (T_{a1}), humidity (q_1), wind (V_{a1}), pressure (p_{a1}), cloudiness (N_{c1}) and precipitation in form of fresh water (P_w) or snow (P_{sn}). At the base of the second oceanic layer ($z_{o2} = 500$ m), temperature (T_{o2}) and salinity (S_2) are prescribed, whereas the geostrophic current (V_{og}) is derived from the mean density structure of the upper 1000 m of the ocean.

Consistent to SLO, the model is run on a spherical, circumpolar grid with a latitudinal resolution of 2.5° and a longitudinal resolution of 5°, extending from 50°S to 80°S. An integration time of 6 years is employed together with a daily time step.

3. Forcing data

Except for the atmospheric temperature, humidity and wind, the forcing is specified from climatologies and essentially identical to that used in SLO for the standard experiment.

To force the SI-OML model with daily variables, analysis results of the data-assimilation phase of an operational NWP model, where actual observations and measurements are included, were employed. In the case of a coarse observing network, the analyses are strongly influenced by the previous forecast (Heimann, personal communication; Trenberth and Olson, 1988). This is advantageous compared to climatological analyses which are purely based on observations. While in the latter case, observation gaps are filled up by spatially and temporally interpolated values, the forecast results are spatially consistent with the patterns of the large-scale circulation and a product of the temporal evolution on the synoptic scale.

The employment of the analysis data as surface forcing fields, however, is generally not uncritical (see, e.g., Cattle and Roberts, 1988), and it must be emphasised that for the Southern Ocean region, these data are primarily simulation results from an atmosphere model, which themselves can be erroneous. Another disadvantage arises because of the continuous improvement of the NWP models parallel to their operational application. Thus, the presently available data sets covering several years, are based on different model versions (Bengtsson and Shukla, 1988) and are consequently not entirely consistent. A third problem, mainly occurring near the ice edge, enters due to the specification of the lower boundary conditions of the employed NWP model (see Subsection 6.1).

In the present study, computations of the global analyses of the European Center for Medium Range Weather Forecasts (ECMWF) were used. They are defined at the standard pressure levels, covering the years 1980–1987, with a resolution of $2.5° \times 2.5°$ in space and 12 h in time (Trenberth and Olson, 1988). From this computational data set, the temperature, relative humidity, wind and geopotential height from the 850 hPa and 1000 hPa pressure levels were extracted for the years 1985 and 1986.

The data were spatially (horizontally) interpolated to the model grid and converted into daily mean values in order to be commensurate with the model time step. For the integration time of six years, the first five years were forced with data from the year 1985, while the sixth year is determined by the 1986 forcing. The model results, which are presented in the following sections, will thus represent this final year of model integration, i.e., the year 1986.

4. Experiments with atmospheric surface forcing

4.1. Forcing configuration

Temperature and humidity at 1000 hPa were interpolated to the surface (or 2 m height) following the ECMWF Research Department (1986), whereas the 1000 hPa winds were used as surface winds without correction for height following Trenberth et al. (1989) and Janssen et al. (1989). The surface pressure was calculated according to Trenberth and Olson (1988).

The purely model-derived, diagnostic atmospheric surface variables archieved in the so-called TOGA data set, also available at the ECMWF, were not employed in the present study. This was mainly due to the fact that these computations, derived during the postprocessing phase, are primarily determined by the ABL processes, which themselves are highly dependent on the specified lower boundary conditions. Over ice covered regions, however, these boundary conditions are rather crude (see Subsection 6.1).

4.2. Results

Using the forcing configuration described above, without any adjustments of the model parameters as compared to the standard version in SLO, the spatial ice-thickness distribution (being the most crucial indicator for the skill of sea-ice simulations) was rather similar to the one obtained with monthly forcing from climatologies

(see Stössel, 1991). The main differences compared to observations were a partially overestimated winter ice extent and a general overestimation of the compression in convergent ice drift areas.

The latter deficiency can be overcome in an ad hoc manner by simultaneously adjusting the sea-ice model parameter P^*, which affects the ice strength (see SLO), and the drag coefficient for the calculation of the wind stress. The reasoning is as follows: In the previous experiment (without adjustments) the 1000 hPa wind, which is assumed to represent the surface wind, was treated as a geostrophic wind with respect to the drag coefficient ($C_{da} = 1.2 \cdot 10^{-3}$). According to McPhee (1980) and Leppäranta (1981), however, this coefficient, when used with surface (or 10 m) winds, should be specified by a ratio 1 to 2 to the corresponding drag coefficient between ice and ocean (C_{do}). Thus, with $C_{do} = 5.5 \cdot 10^{-3}$ it follows that $C_{da} = 2.7 \cdot 10^{-3}$ for the 10 m wind (see also Overland, 1985). Since, with such a modification, the ice is expected to encounter too much ridging in convergent ice drift regions, the ice-strength

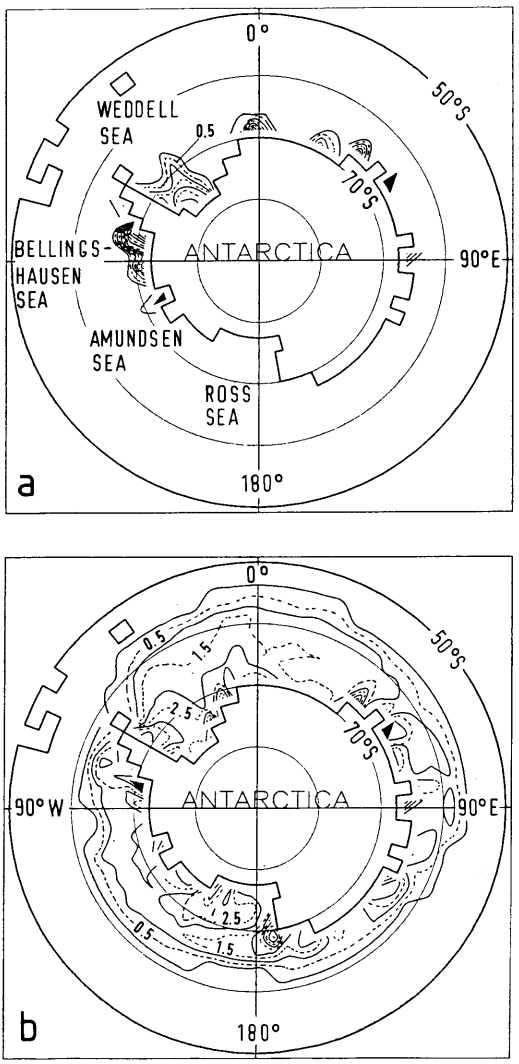

Fig. 2. Ice-thickness contours (increment: 0.5 m) simulated with the SI-OML model with conventionally adjusted ice strength and surface stress, representing the approximate dates of (a) minimum (1 March 1986) and (b) maximum (27 September 1986) ice extent.

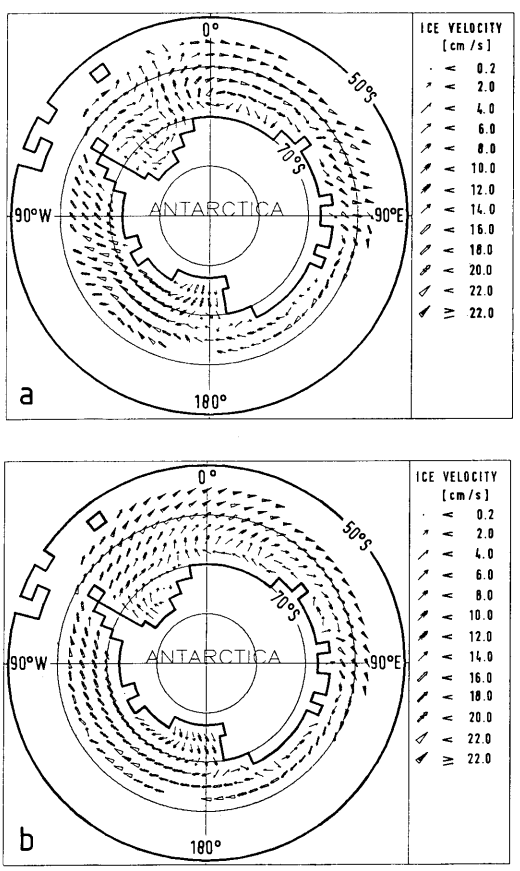

Fig. 3. Ice velocities (increment: 2 cm/s) from the same model version as in Fig. 2, for (a) the approximate date of maximum ice extent (27 September 1986) and (b) the monthly mean of September 1986.

parameter, too, was increased by a factor of 5.5 proposed by Hibler and Ackley (1983) for the application of daily wind forcing (see SLO).

The resultant ice-thickness distribution is shown in Fig. 2 for the approximate date of minimum (a) and maximum (b) ice extent. The most significant difference to the earlier result without adjustment (Stössel, 1991: Fig. 1), is the highly reduced ridging in convergent ice drift areas, where the increased ice strength exerts a higher effect than the increased stress between the ice and the atmosphere.

Fig. 3a shows the corresponding ice drift in winter for 27 September 1986, i.e., for an instantaneous date, while Fig. 3b represents the monthly mean of this variable for September 1986. In the daily plot, the ice drift is dominated by an extensive anticyclonic gyre in the Weddell Sea. Ice velocities of almost 30 cm/s are achieved even in compact, but divergent, ice fields (Amundsen Sea at 70° S), approaching values of free ice drift. The structure of the monthly mean ice drift (Fig. 3b) corresponds essentially to the (reasonable) results obtained with the standard experiment with climatological (monthly mean) forcing in SLO, with the characteristic (cyclonic) Weddell gyre, the strong offshore ice drift in the Ross Sea and several smaller gyres along the coast of East Antarctica.

Fig. 4 shows the contours of the mixed-layer depth and corresponds to Fig. 5 in SLO. The equilibrium depth of the mixed layer in summer (Fig. 4a), which is determined by the Monin-Obukhov length, increases to about twice the amount registered with the monthly mean wind forcing (compare with Fig. 5a in SLO). In winter, the mixed-layer depth is deeper by about 40 m compared to the earlier results, and thus in

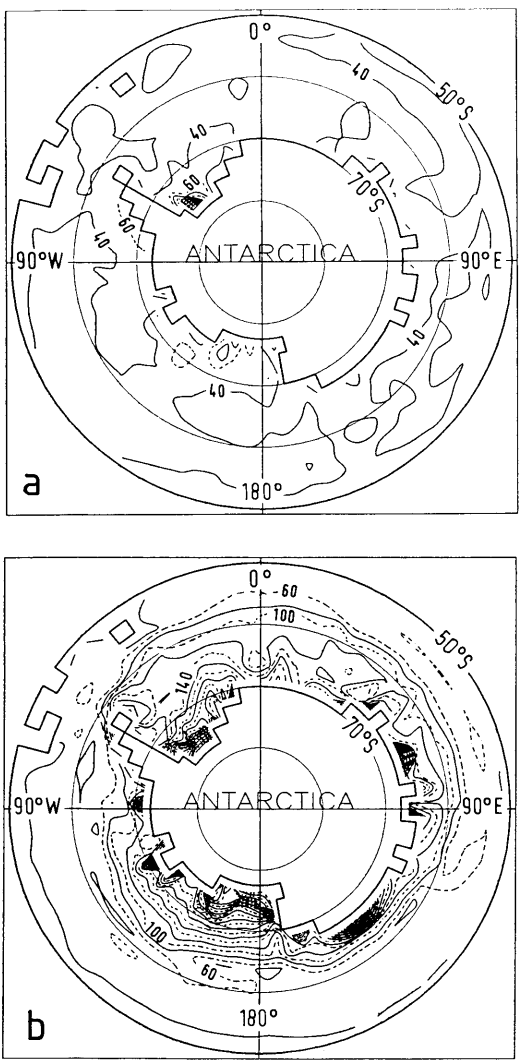

Fig. 4. Contours of oceanic mixed-layer depth (increment: 20 m) from the same model version and for the same dates as in Fig. 2.

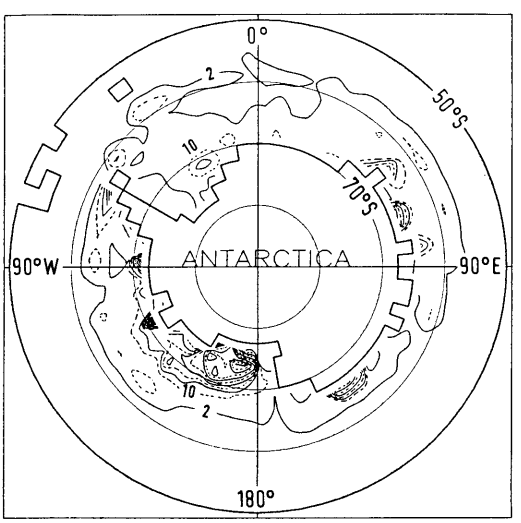

Fig. 5. Contours of the monthly mean vertical oceanic heat flux (increment: 8 W/m^2, minimum contour line: 2 W/m^2) for August 1986 from the same model version as in Fig. 2.

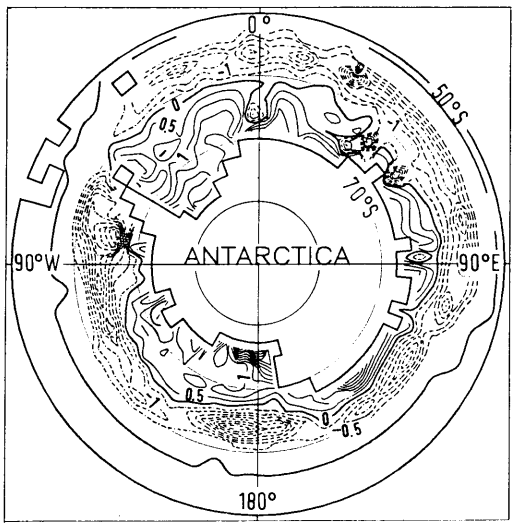

Fig. 6. Net freezing rate in equivalent meters of ice thickness (increment: 0.5 m) for the sixth simulation year of the same model version as in Fig. 2. The broken lines (negative) represent more melting than freezing, the thin, full lines the opposite.

remarkably good agreement with local observations (Martinson, 1990; Gordon and Huber, 1990). New areas of deeper mixed layers occur in the Bellingshausen and Amundsen Seas.

Compared to the climatologically forced experiment (SLO: Fig. 6), differences in the pattern of the mean oceanic heat flux (Fig. 5) in August are restricted to single locations, whereas the magnitude has globally increased by about a factor of four. The area of positive net freezing rate has expanded considerably to the north in the Weddell Sea as well as in the Ross Sea (Fig. 6 versus Fig. 13 in SLO) and the local melt rates are strongly increased.

5. Extension with ASL model

5.1. Model and forcing configuration

In the previous section, an example of traditional adjustment practices in terms of model parameters and drag coefficients was given. In order to establish such modifications on a more physical basis, the effects of static stability in the ASL are in the following incorporated in terms of an interactive modification of the atmospheric forcing.

As mentioned earlier, in the Southern Ocean region the applied analysis data are primarily model derived. Since the standard pressure levels of the ECMWF analyses do not coincide with the vertical grid of the correspondent NWP model (where the lowest level represents a height of about 30 m), the computations were accordingly interpolated during the assimilation phase (ECMWF Research Department, 1986; see also Heimann and Monfray, 1989).

Recalculating these variables to the lowest NWP model level in the case where the 1000 hPa level lies below that model level, and otherwise using the original 1000 hPa values together with their instantaneous height, the turbulent heat fluxes (transfer coefficients) and the stress over ice (drag coefficient) can be determined via the employment of an ASL parameterisation. This parameterisation corresponds to the one employed in the NWP (atmospheric general circulation [AGC]) model of the ECMWF (ECMWF Research Department, 1985; Louis, 1979) and is based on the Monin-Obukhov theory. In the present application the height of the lowest atmospheric layer varies according to the height at which the forcing variables are prescribed (as noted above).

The vertical eddy fluxes of momentum and heat are dependent on stability functions, which for neutral and convective stratifications follow from analytical adaptations to the functions of Businger et al. (1971). In the case of highly stable stratifications, the stability functions are allowed to approach an asymptote in order to avoid an energetic disconnection of the surface from the atmosphere (Louis, 1979). The application of the ASL scheme implies horizontal homogeneity. Thus, it is implicitly assumed that the surface layers develop separately over the ice free and the ice covered part of a grid cell. Due to the seven-level ice-thickness parameterisation, incorporated in accordance to Hibler (1984) (see SLO), the ASL is additionally assumed to equilibrate separately over each of the seven equally distributed ice-thickness categories.

In accordance to the ECMWF model, the roughness length over sea ice (z_{si}) is $1 \cdot 10^{-3}$ m and that over ice-free waters (z_{so}) is determined by Charnock's formula ($z_{so} = Cu_*^2/g$), i.e., via the

instantaneous friction velocity (u_*), the acceleration due to gravity (g), and the Charnock constant ($C = 0.032$).

The ice-strength parameter P^* (modified in the experiment described in Section 4) is reset to the original value (Hibler, 1979), which was also used in the standard case in SLO.

5.2. *Results*

Fig. 7 shows the resulting ice-thickness distribution for the same dates as in Fig. 2. In spite of the low P^*-value the results are rather similar to the ones of the previous experiment (Fig. 2). Contrary to the latter, convergent drift regions are somewhat more pronounced, leading to more multi-year ice, especially in the Ross and Amundsen Seas (which is evident from the summer distribution shown in Fig. 7a). Complementary, the monthly mean ice velocities are reduced, especially in divergent ice fields (Fig. 8). These features represent a significant improvement towards observations.

In comparison to the previous results (Fig. 4), the summer mixed-layer depth (Fig. 9a) is generally reduced by 10–20 m, while the winter mixed-layer depth differs only at several locations along the coast (especially in the southern Weddell Sea and in the south-eastern Ross Sea).

On the large-scale, ice compactness is easier to verify. Its simulated real-time areal distribution for the year 1986 is demonstrated in Fig. 10 in 3 months intervals. Fig. 11 presents slightly modified copies of operational ice charts (Naval Polar Oceanography Center, 1986), which are based on real-time observations from a variety of sources. The scale and dates are consistent with Fig. 10. The summer ice extent, which usually is the most difficult one to simulate, is reasonable within the limits of the model resolution (Fig. 10a). The period of ice advance (Fig. 10b) and the winter ice compactness (Fig. 10c) are well simulated, although the extent is overestimated in some sectors. The high concentrations ($N_i > 80\%$) beyond

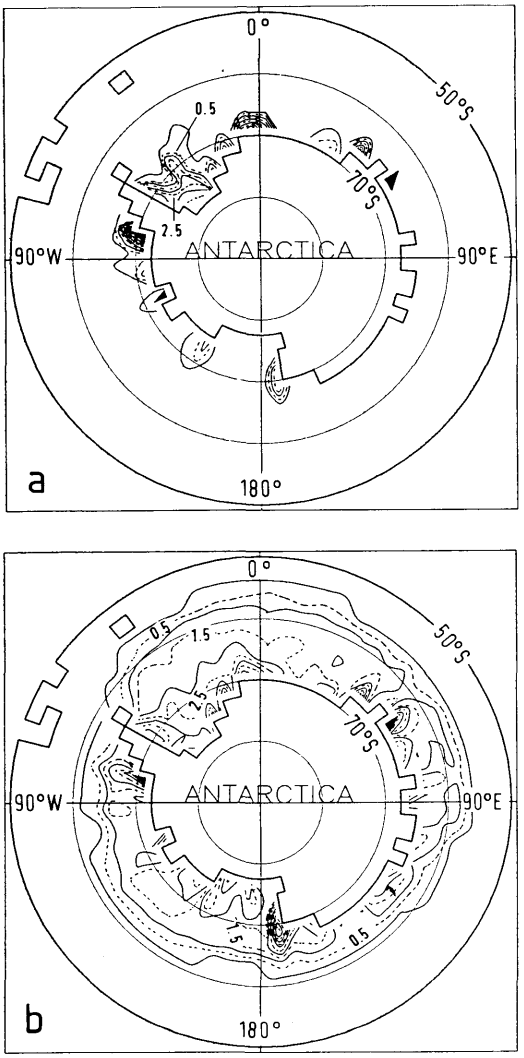

Fig. 7. Ice-thickness contours simulated with the ASL-SI-OML model, otherwise like Fig. 2.

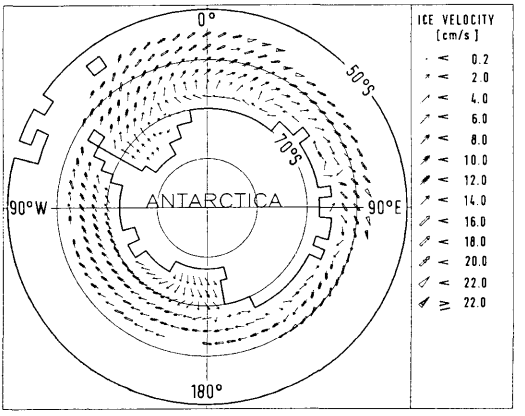

Fig. 8. Monthly mean ice velocities from the same model version as in Fig. 7, otherwise like Fig. 3b.

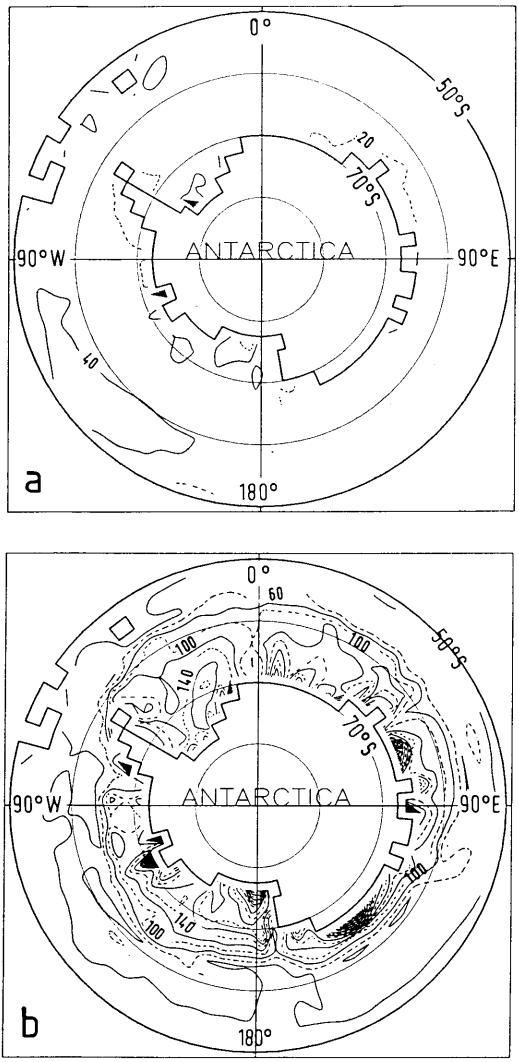

Fig. 9. Contours of oceanic mixed-layer depth from the same model version as in Fig. 7, otherwise like Fig. 4.

the marginal ice zone (MIZ), as well as its width compare well with observations (Figs. 11b and 11c; see also Wadhams et al., 1987). The process of ice break-up in spring (Fig. 10d), starting in the Indian Ocean sector, is also captured by the model as can be verified by Fig. 11d. Coastal polynyas can be identified by lower concentrations along the continent. The observed polynya in the southern Ross Sea is not present in the simulation. Instead, there is a polynya in the eastern Ross Sea, which can be attributed to an increased vertical oceanic heat flux due to instantaneous divergent ice drift with simultaneous cold-air advection (from the mainland).

6. Extension with ABL model

6.1. Model and forcing configuration

A drawback of using analysis data from NWP centers as forcing data is the fact that these are influenced by the lower boundary conditions of the operational AGC model, which in the present case are given by climatological ice surface temperatures beyond the essentially climatologically determined ice edge (ECMWF Research Department, 1986). To circumvent this deficiency and to modify the forcing by Ekman layer physics, an attempt was made to raise the forcing level with respect to temperature, humidity and wind to the next higher one of the (ECMWF) analyses (850 hPa). This is in the following achieved by an additional coupling to a one-dimensional ABL model, as was done by Koch (1988) for the Weddell Sea-ice model of Hibler and Ackley (1983).

In the ABL model, the surface layer is treated in accordance to the Monin-Obukhov similarity theory, i.e., similar to the ASL parameterisation described in the previous section. The Ekman layer is resolved using the Rossby-number similarity theory. Vertical integration of the flux-profiles from the roughness length z_s to the geostrophic level z_{a2} yields the resistance laws for the barotropic Ekman layer (Koch, 1988). The friction velocity and the turbulent heat fluxes are related to empirically determined stability functions (Fiedler and Panofsky, 1972), which depend on the stability parameter $\mu = (\kappa u_*)/(fL)$, where κ is the von Karman constant, f the Coriolis parameter and L the Monin-Obukhov length. Additionally, the similarity theory provides the turning angle between the geostrophic flow and the stress at the surface.

As with the ASL parameterisation, the application of the ABL scheme assumes horizontal homogeneity (see Subsection 5.1), leading to separate developments of the ABL over the ice free part and seven ice-thickness categories over the ice covered part of a grid cell.

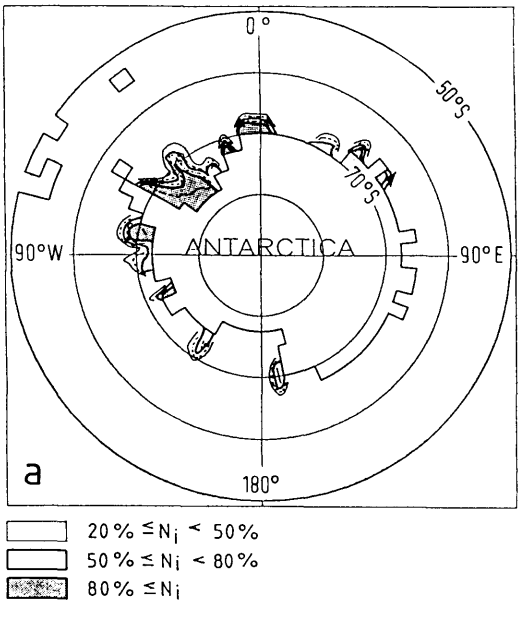

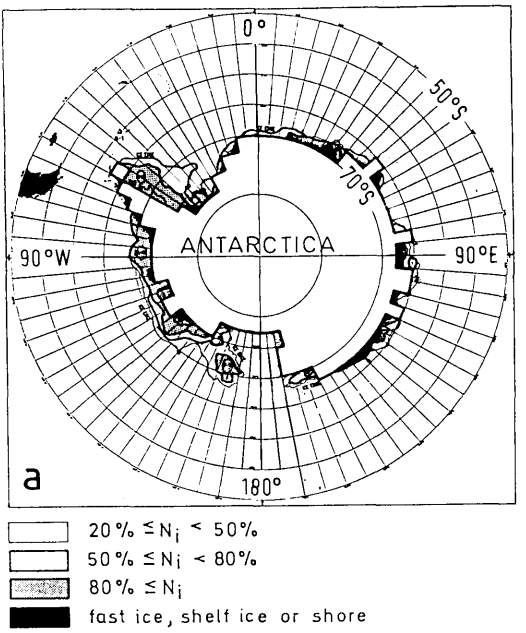

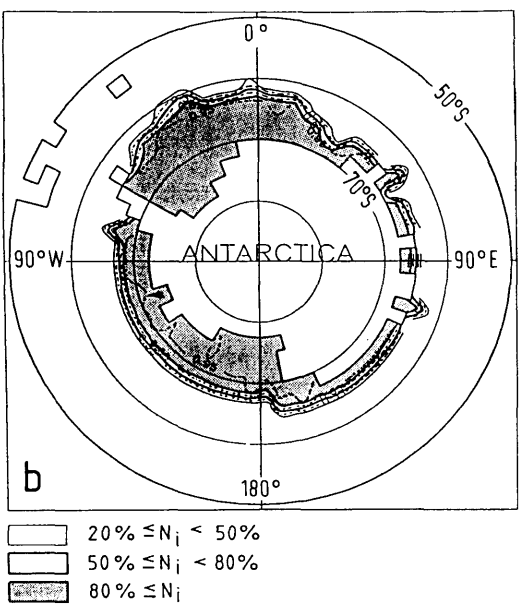

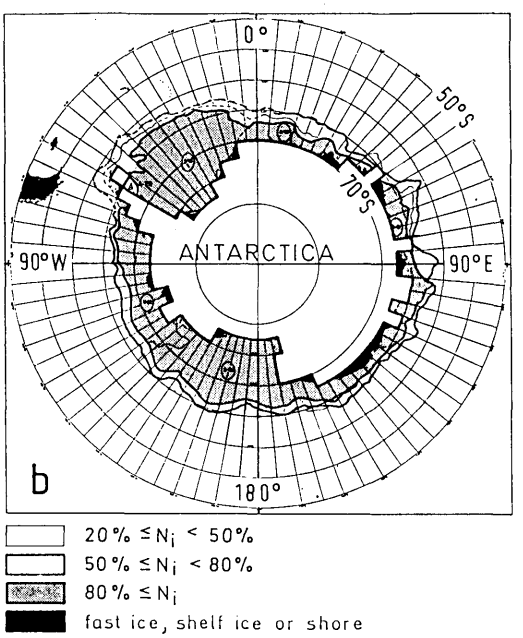

Fig. 10. Contours of the real-time ice concentration from the same model version as in Fig. 7, representing (a) 27 February 1986, (b) 29 May 1986, (c) 28 August 1986 and (d) 26 November 1986.

Fig. 11. Contours of the real-time ice concentrations according to the Navy/NOAA Joint Ice Center based on observations and satellite data, otherwise like Fig. 10.

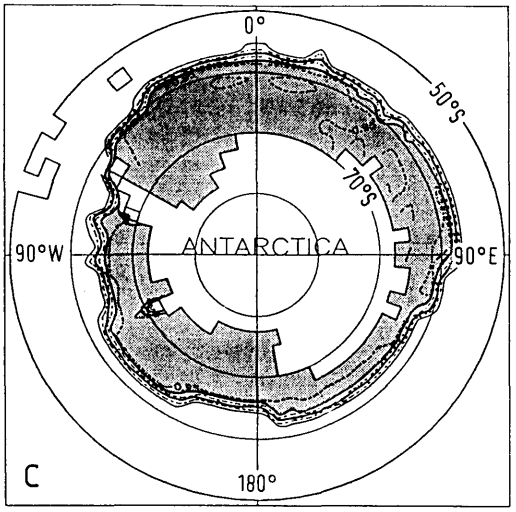

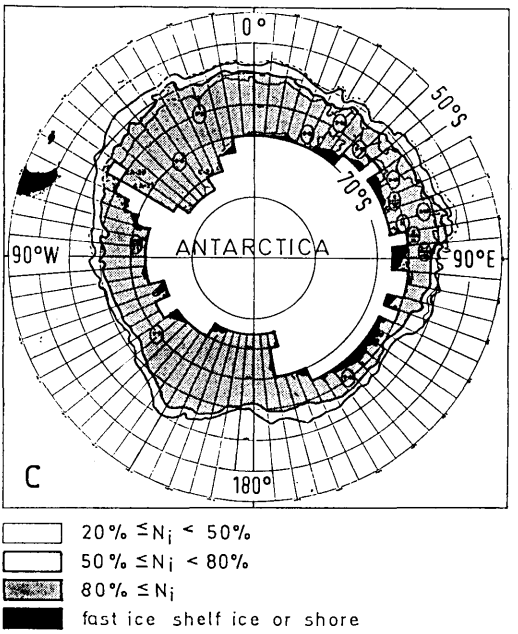

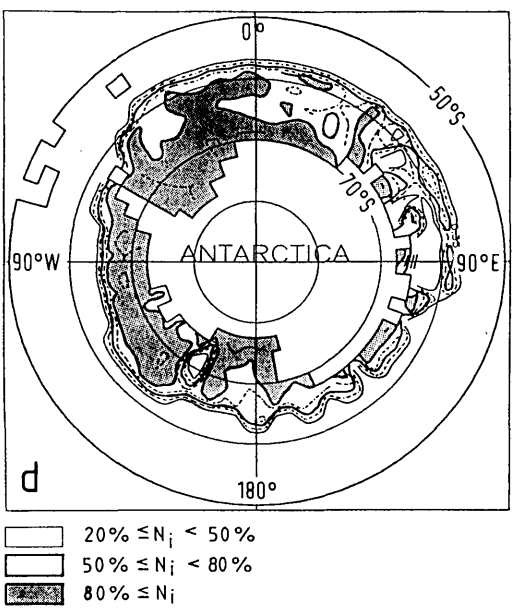

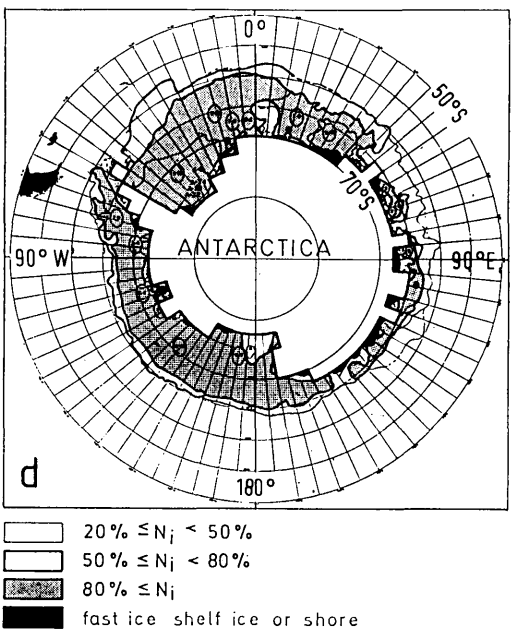

Fig. 10. Continued.

Fig. 11. Continued.

6.2. Results

6.2.1. Preceding experiments. Using the original parameters of both the ABL (Koch, 1988) and the SI-OML model, the results of the coupled ABL-SI-OML model were not promising (see Stössel, 1991, Fig. 2). Specifically, the ice extent was significantly reduced compared to the standard results of the SI-OML model. Additionally, the ice-thickness distribution showed a more or less zonal pattern, indicating a severe underestimation of the ice velocities in the compact ice field.

It was shown in Stössel (1991) that the characteristic ice-thickness distribution was not achieved, unless the lowermost (1000 hPa) wind field was used to drive the sea-ice model dynamically. This was identified to be due to the naturally weakened orographic impacts on the 850 hPa wind fields as compared to the 1000 hPa ones. As was pointed out, however, even in large-scale sea-ice simulations it is essential to have orographic features like katabatic and barrier winds included in the wind forcing in order to achieve reasonable sea-ice characteristics off the coast of Antarctica (see also Schwerdtfeger, 1979). Thus, for the following experiments, the use of the higher-level winds has been withdrawn, thereby restricting the higher-level forcing to the temperature and humidity fields only. It will be shown in the following that under this configuration the results can be improved while retaining the original formalisms of the models.

6.2.2. Sensitivity to roughness length. According to Koch (1988), the roughness length over ice was specified as $z_{si} = 2 \cdot 10^{-4}$ m. This is twice the value for ice free water surfaces ($z_{so} = 1 \cdot 10^{-4}$ m) and is usually taken as the local roughness length for smooth ice surfaces (skin drag) (Hanssen-Bauer and Gjessing, 1988; Claussen, 1991). The latter, however, is not consistent with observations of Southern Ocean pack ice, which rather consists of a random mixture of inhomogeneous features like leads, pressure ridges and floes of different size and freeboard (Wadhams et al., 1987). Thus, it seems to be adequate for the present large-scale simulation to consider these surface structures by adding a so-called form drag to the skin drag mentioned above (Arya, 1975), which corresponds to an effective increase of the roughness length over ice by 2 orders of magnitude (Hanssen-Bauer and Gjessing, 1988).

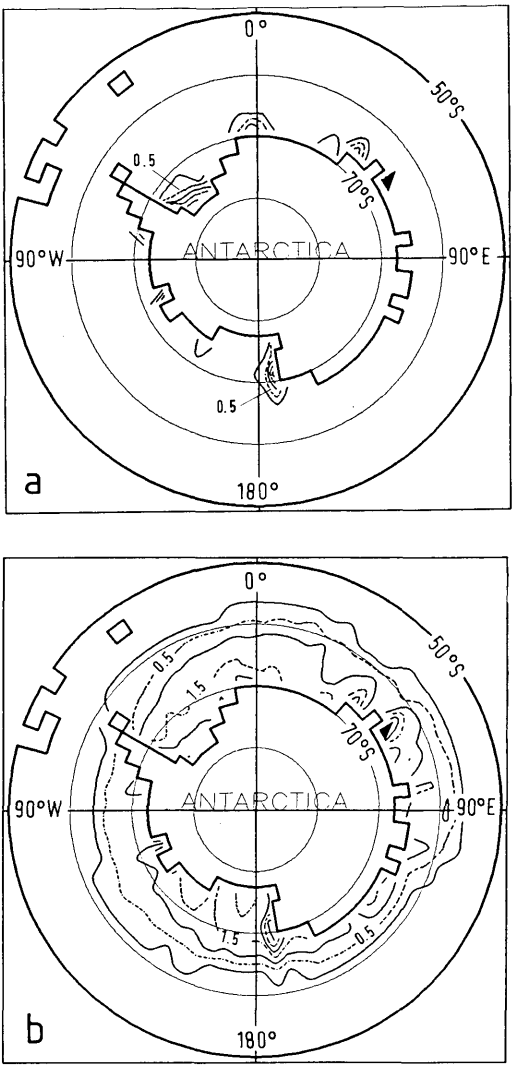

Fig. 12. Ice-thickness contours as simulated with the ABL-SI-OML model employing the 1000 hPa winds and a higher surface roughness, otherwise like Fig. 2.

The kinetic energy input into the mixed layer is calculated via the ice velocity, which in grid cells without ice (zero ice mass) is essentially determined by the air drag. In the present case with ABL coupling the latter is determined via the stability-dependent friction velocity, which in an ice free grid cell depends on the roughness length

over open water (z_{so}). In order to achieve energetical consistency with the kinetic energy input of the SI-OML model without boundary-layer algorithms (where the drag over ice and water was the same), z_{so} is also raised by 2 orders of magnitude. It is noticed that this specification differs from the corresponding one of Section 5 (see 5.1).

As is evident from Fig. 12, this measure leads to a significantly improved ice extent as compared to the preliminary results of the ABL-SI-OML model (Stössel, 1991: Fig. 2). The characteristic ice-thickness distribution (as demonstrated in Figs. 2 and 7), however, is not captured. Specifically, the rather zonal ice-thickness distribution indicates that the higher roughness length over ice hardly has any impact on the locally computed friction velocity (and thus on the air/ice stress).

This feature becomes obvious in a further experiment where the roughness length over open water is reset to the original (lower) value: the result is nearly unchanged compared to the control run, where both z_{si} and z_{so} have the lower values. Thus, the improvement of the results is attributed to the increased roughness length over open water. This was found to be due to higher turbulent heat fluxes, leading to stronger cooling and higher growth rates of new ice.

6.2.3. Ratio of drag coefficients. Another sensitive parameter in the coupled ABL-SI-OML model is the oceanic drag coefficient, C_{do}. According to McPhee (1980), the proper choice of this parameter is primarily determined by its ratio to the corresponding coefficient between ice and atmosphere, C_{da} (see Section 4), which varies between 2.0 and 1.4 depending on author and region (McPhee, 1980; Leppäranta, 1981; Hoeber and Gube-Lehnhardt, 1987). Since in the ABL model C_{da} is variable (being calculated via the friction velocity: $C_{da} = u_*^2/|V_{a1}|^2$), C_{do} would have to be treated as a variable as well, in order to keep the ratio of the two coefficients fixed. Such an experiment, however, yielded unrealistic results in the form of a severe overestimation of the drift rates in the divergent field. A reduction of C_{do}, e.g., to half the original value, on the other hand, provided much more realistic results (not shown).

6.2.4. Influence of wind turning. Another variable of the ABL model which depends on the roughness length is the turning angle of the wind in the Ekman layer. As mentioned before, the roughness length over ice in the AGC model of the ECMWF is specified as 0.001 m. In a variety of ice situations, this value seems to be underestimated by one order of magnitude. In the present ABL-SI-OML model, on the other hand, an increase of z_{si} by one order of magnitude leads to differences in the turning angle of up to 15°.

For the Antarctic region, similar studies were conducted by Mitchell and Senior (1989) with the

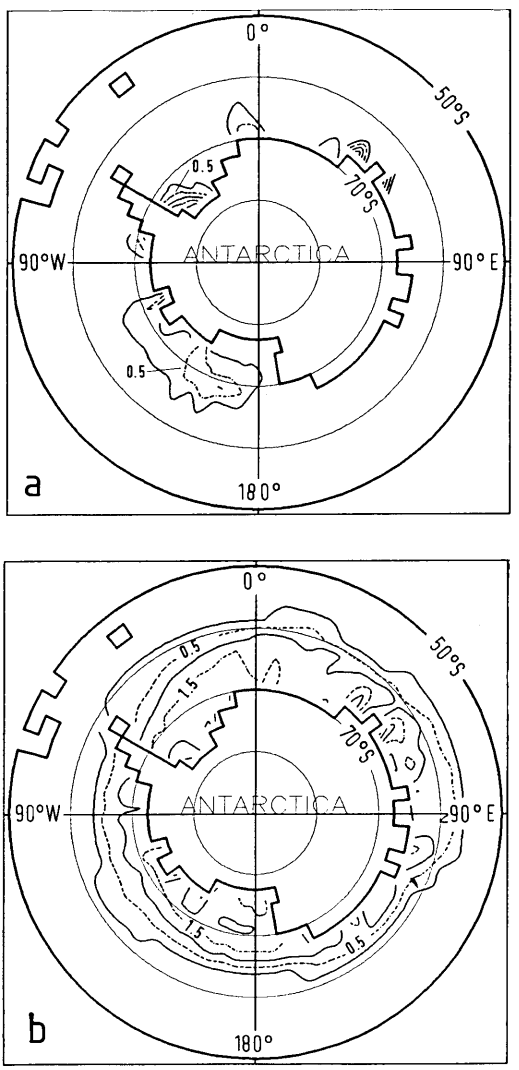

Fig. 13. Ice-thickness contours from the same model version as in Fig. 12, with employment of additional wind turning, otherwise like Fig. 2.

AGC model of the United Kingdom Meteorological Office (UKMO). The motivation for their study was the investigation of the sensitivity of the AGC model to different ice extents. They reduced the large-scale surface roughness over ice covered regions by 3 orders of magnitude and examined this effect separately from the other influences of sea ice (surface temperature, albedo, etc.). In the lower layers of the higher latitudes this measure yielded a reduction of the turning from the circumpolar westwinds to higher latitudes, where it induced a lowering of the surface pressure.

To inversely investigate the impact of this effect on the ice, the 1000 hPa winds are treated as geostrophic winds with respect to the wind turning in the following experiment (Fig. 13). This can be justified by the assumption that the lower-level winds in the AGC model of the ECMWF are turned too weakly due to the presumably underestimated roughness length over ice. Otherwise, the experiment is analogous to the first one in Subsection 6.2.2 (Fig. 12). Except for local differences in the winter ice-thickness distribution as compared to Fig. 12, the most striking feature is a distinct ice tongue in the eastern Ross Sea in summer, being a significant improvement towards observations (see Fig. 11a; Jacobs and Comiso, 1989).

6.2.5. Increase of buoyancy fluxes. So far, it was assumed that the dynamic forcing of the oceanic mixed layer and of the sea ice is dependent on the separately calculated local friction velocity (and thus on the local stability). In the following an experiment was carried out, where only one single ice-concentration weighted friction velocity for the entire grid cell was employed. Although the ice became more mobile in the MIZ, the effect of the modification was negligible in the major part of the ice pack.

A more realistic result was achieved by (exaggeratedly) employing the drag calculated over the ice free part for the dynamic forcing of the sea ice. A correspondent experiment clearly yielded the characteristic ice-thickness distribution (not shown). However, as expected, the ice ridging in convergent drift regions was severely overestimated, implying that the appropriate magnitude of the grid-cell averaged air/ice stress for the ABL-SI-OML model is somewhere in between both extreme cases described here.

6.2.6. Interannual variation. In the experiment with the ASL-SI-OML model, where the atmospheric thermal forcing was derived from the lower (1000 hPa) level of the global analyses, it was not possible to simulate the interannual variation of ice extent between 1985 and 1986, as is obvious from the winter ice extent in 1986 (Fig. 14, dashed curves). The ABL-SI-OML model, with the thermal forcing from the 850 hPa level, on the other hand, captures the relative variation between both years quite realistically (Fig. 14, full curves), as can be verified against the correspondent seasonal cycles derived from satelliteborne radiometer data (Gloersen and Campbell, 1988) (Fig. 14, dotted curves). Taking advantage of the previous experiments with additional wind turning and increased buoyancy fluxes, even the absolute value with respect to the winter maximum is about correct.

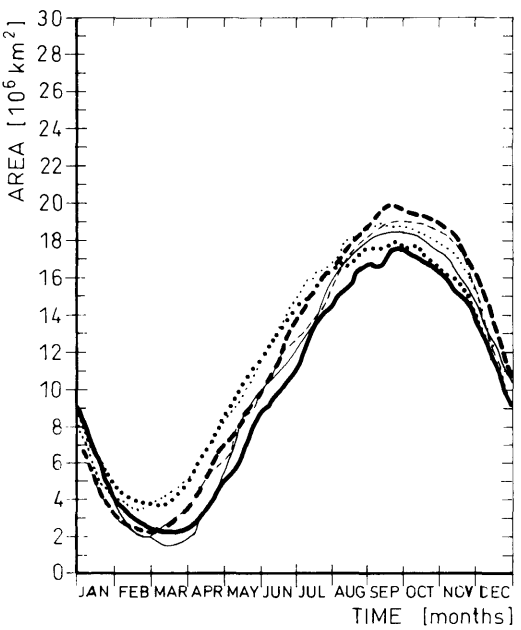

Fig. 14. Seasonal cycles of ice extent derived from SMMR data according to Gloersen and Campbell (1988) (dotted curves), simulated with the ASL-SI-OML model (dashed curves) and simulated with the ABL-SI-OML model, employing additional wind turning and increased buoyancy fluxes (full curves), for 1985 (thin curves) and 1986 (thick curves), respectively.

7. Summary and discussion

With the presently employed atmospheric forcing the results were (in first order) promising, thus generally supporting the reliability of the ECMWF analyses. Applying conventional adjustment to the changed forcing, improved the results with respect to reduced ridging in convergent ice drift regions (Fig. 2). The higher wind variability and the larger drag coefficient led to a higher ice drift (Fig. 3) and thus to an increased turbulent kinetic energy input into the ocean, which modified the mixed-layer depths (Fig. 4) and the entrainment heat flux (Fig. 5) to closer agreement with observations. The changes in the pattern of the net freezing rate (Fig. 6) are on the one hand related to the higher turbulent heat fluxes resulting from the increased wind variability and, on the other hand, to more frequent occasions for new-ice production in winter resulting from the correspondent higher variability of ice drift.

The main deficiency of the results with atmospheric surface forcing was the overestimation of ice drift in compact, divergent ice fields. This is related to the impact of the change of the ice-strength parameter, which essentially modifies the simulation in convergent ice drift areas with high ice compactness and thickness. Altering the wind forcing from monthly mean values to daily ones, however, also affects the divergent parts of the ice pack, which in the Southern Ocean region are dominating.

Modifying the forcing fields by the introduction of an ASL parameterisation improved the ice-thickness distribution (Fig. 7) and especially the ice velocities in the divergent ice areas (Fig. 8). The latter feature is due to the fact that the ASL parameterisation provides stable stratifications over thick and/or snow covered ice, thereby reducing the strength of the momentum forcing.

With the employment of the ASL parameterisation, the changes in mixed-layer depths (Fig. 9) are related to the specification of the roughness length in summer (discussed below) and to the reduced ice drift in winter. The latter leads to a reduction of the momentum transfer between sea ice and ocean, which finally reduces the mixed-layer depths. The differences in the winter mixed-layer depths (Fig. 4b versus Fig. 9b) being restricted to locations of ice divergence (compare with Fig. 3b), indicates that these locations were not particularly modified by the higher P^* value in the experiment of Section 4. Specifically, while in convergent regions the reduced ice strength and the effectively reduced drag coefficient seem to balance each other, this is not so in divergent regions, where the effect of the reduced drag coefficient is larger than the effect of reduced ice strength. This again indicates that P^* is not the appropriate adjustment parameter for the overall ice pack if the variability of the wind forcing is changed.

A large-scale verification of the results was provided by comparing the real-time spatial and temporal distribution of the ice compactness (Figs. 10) with corresponding observation products (Figs. 11), showing general consensus except for local overestimations of winter ice extent, and the spring-time polynya and summer ice extent in the eastern Ross Sea.

The dependency on the specified (climatological) boundary conditions of the NWP model was reduced by raising the dominant atmospheric forcing to the geostrophic level and employing an ABL model. Based on preceding simulation experiences (Stössel, 1991), the upper level forcing was restricted to the thermal variables.

One candidate for the earlier disagreement with observations was the inconsistent specification of the roughness lengths over the ice covered as well as over the ice free part of the ocean. The improvement of the results with an increase of both roughness lengths by two orders of magnitude (Fig. 12) was primarily attributed to the increased roughness length over open water, leading to enhanced new-ice production.

In this context, the reduction of the summer mixed-layer depths resulting from the experiment employing the ASL parameterisation (Section 5; Fig. 9a as compared to Fig. 4a) is largely related to the fact that in an ice free grid cell the turbulent kinetic energy transfer was determined via a z_{so}, which itself was dependent on the Charnock constant and the instantaneous friction velocity (see Subsection 5.1). This yields a roughness length which is generally 2 to 3 orders of magnitude lower than the specified value of $z_{si} = 1 \cdot 10^{-3}$ m. In order to provide a smooth transition of kinetic energy input from ice-free to ice-covered grid cells (across the MIZ), an ice-concentration weighted contribution of the ice drift ("ice keel stirring") seems to be reasonable.

In Section 4, the larger mixed-layer depths (as

compared to SLO and Section 5) are due to the higher turbulent kinetic energy input depending on a constant drag coefficient ($C_{da} = 2.7 \cdot 10^{-3}$, which is equal for the ice covered and open water part). On the other hand, an enhanced cooling of the mixed layer (as achieved in the simulation with both z_{so} and z_{si} raised by 2 orders of magnitude) was not induced, because (in terms of bulk formulas) the change of the drag coefficient has no influence on the calculation of the turbulent heat fluxes (which are rather dependent on the so-called transfer coefficients).

The ratio of the respective drag coefficients, too, is a sensitive quantity with respect to the consistency in momentum transfer between atmosphere, sea ice and ocean. The failure of the experiment with the oceanic drag coefficient depending on the (variable) atmospheric friction velocity is due to the fact that the friction effect of the ocean on the ice (generally in form of a negative acceleration) becomes negligible below a critical value of the air drag (generally during strong stable stratification in the ABL). This implies that if one of the drag coefficients is treated as a function of the ambient, instantaneous conditions, the ratio concept is not appropriate for all situations.

For smooth and compact ice fields, the additionally specified wind turning (Fig. 13) appears to be overestimated. However, its effect is suppressed by the high static stability in the ABL prevailing over such fields. In the MIZ, on the other hand, it can be assumed that the roughness is much higher due to the lower ice concentration (Andreas et al., 1984; Mitchell and Senior, 1989). Additionally, during spring and summer, the stratification of the ABL becomes less stable, thus increasing the strength of the coupling between atmosphere and sea ice. This leads to a higher effectiveness of the additional wind turning and finally to the improved results, indicating that the lower boundary conditions in the AGC model might be inadequately specified in those areas.

With the ABL-SI-OML model, the characteristic ice-thickness distribution was achieved after a drastic increase of the buoyancy fluxes. The ice-concentration weighted determination of the surface stress not being very effective, infers that the dynamic decoupling of the atmosphere from the sea ice (induced by the ABL model during stable stratifications) is too strong. With respect to this feature, snow cover, too, is a crucial factor, since it isolates the atmosphere from the ocean more than sea ice alone. On the other hand, it is noted that the large-scale destabilising influence of leads on the stratification of the ABL is generally non-linearly weighted with the ice concentration. The turbulent heat fluxes, e.g., are inversely proportional to the downwind fetch over a lead (Worby and Allison, 1991). Experiments including such considerations, especially in terms of a large-scale roughness length for inhomogeneous ice distributions within a grid cell, are in preparation.

The failure to simulate interannual variation with thermal forcing from the lower analyses level (Fig. 14) indicates the influence of the lower boundary conditions of the AGC model. Since the year 1986 was rather anomalous in the sense that the winter maximum ice extent was far below the climatological value (Gloersen and Campbell, 1988), the prescribed climatological treatment of the MIZ in the AGC model (see Subsection 6.1) yielded colder than observed temperatures in the lowest level of the AGC model, thus explaining the local discrepancies in maximum ice extent of 1986 (e.g., Fig. 10c versus 11c). This indicates that in areas of high interannual variability, as is the case around the ice edge, it is important to relax the climatological component of the prescribed boundary conditions more toward the instantaneous conditions in order to make the near-surface analysis data over that region more representative for the respective years.

Using the ABL-SI-OML model, the ice extent in the Weddell Sea is generally underestimated (relative to the other parts of the model domain). This failure is related to the one-dimensional description of the ABL model, not being capable to solve the advective features in that region. Generally, cold air advects into the western and northern parts of the Weddell Sea below the inversion. A compensating warm-air advection from the west-wind zone towards higher latitudes exists at higher levels (Schwerdtfeger, 1984). These advection processes are mainly responsible for the extreme vertical potential temperature gradients observed over major parts of the Weddell Sea, not being captured by the present ABL model and consequently leading to higher than observed surface air temperatures.

Analogous features are to be expected in the oceanic part (not captured by the one-dimensional

OML model), where the situation is complicated by the northward transport of fresh water at the surface (ice drift + ice melt) and by the topography of the continental shelf. Specifically, advection of warmer water onto the shelf region, induced by upwelling processes at the continental slope, may occur, compensating the sinking of colder and more saline water produced over the shelf primarily by new-ice formation. This is especially observed over the continental shelf of the Ross Sea, where the ice concentration in winter is generally lower than over the deep sea (Jacobs and Comiso, 1989).

8. Conclusions and further requirements

Three major aspects concerning the coupling of atmosphere, sea ice and ocean were stressed in this paper. Firstly, blended observation/simulation products were employed as atmospheric forcing. Secondly, modifications of the strength of the atmospheric forcing by considering boundary-layer physics were introduced. Finally, sea ice has been used as the experiment agent by mens of a highly sophisticated large-scale sea-ice model. All three aspects lead to useful implications for coupled AGC-SI-OGC models, being summarised in the following.

Noticing the remote location of the Southern Ocean with its coarse observational network, the results of the SI-OML model forced with variables of the ECMWF analyses were encouraging. The introduction of daily wind variability, too, improved the results (e.g., rate of new-ice production, mixed-layer depth and oceanic heat flux). Inconsistencies, obviously arising from the analyses, were detected to be primarily due to inadequately specified boundary conditions in sea-ice region in the ECMWF AGC model (e.g., climatological ice edge, no fractional ice coverage, partly underestimated roughness length over sea ice). At locations where inconsistencies arise, a careful analysis is required by means of adjusting the unknown parameters of both the model which generates the forcing fields, and the model which is forced.

Concerning the modification of the forcing strength by including boundary-layer considerations, the first intention was to incorporate the weakening of the heat, mass and momentum fluxes due to stable stratifications usually occuring over thicker and/or snow covered sea ice. This is different from the usual bulk formulations, where the flux increases linearly with the vertical gradient. Simultaneously, it was intended to include the effect of the instantaneous (simulated) surface (sea-ice) conditions. This is again different from the usual way of modifying the fluxes (e.g., for ocean modelling or wave modelling), where stability effects are determined from the variables of the same (climatological) data set from which the primary forcing data are derived. Thus, e.g., with regard to the momentum transfer between atmosphere and open ocean, the variation in surface roughness (expressed by the Charnock formulation) is instantaneously accounted for, while the variation in the stability of the ABL is climatological. In areas with sea-ice occurrence, however, both variations have to be considered instantaneously in order to provide a reasonable forcing.

Indeed, while traditional adjustment methods partly failed, the described modification via the ASL parameterisation yielded more promising simulation results (e.g., amount of ridging, ice velocities). With the thermal forcing raised to the geostrophic level (ABL model), further sensitive terms crucial for the coupling of the three spheres were identified (e.g., the kinetic energy input into the ocean via the respective roughness lengths or drag coefficients), implying that the correct heat, mass and momentum transfer between atmosphere and ocean via sea ice is more related to the ratio of the respective parameters than to their absolute values, inferring the coupling problem to be essentially determined by a consistency problem.

The presently used vertical ABL description appeared to be unsuitable for certain conditions (e.g., too strong dynamical decoupling at stable stratifications, uncapable to overcome high vertical gradients). With regard to the decoupling at stable stratifications, the integrated, large-scale buoyancy flux over a partly ice-covered grid cell, too, is an unsolved problem, which is especially important for coupled AGC-SI-OGC models. Since on these scales, floe and lead size resolving SI models will probably not be used within the immediate future, the averaged buoyancy flux has to be parameterised in terms of the instantaneously simulated large-scale ice concentration and ice thickness. This can only be achieved by incorporating sub-grid scale boundary-layer

processes, which adjust interactively to current variations in sea-ice conditions.

In coupled AGC-SI-OGC models the results of the sea-ice part are determined by the deficit of energy at the atmosphere-ocean interface. An accurate determination of this deficit can only be guaranteed if the heat, mass and momentum transfer between atmosphere and ocean is consistent with the comprehensive physics of sea ice. In this sense, it is equivalently important for the potential energy (e.g., in form of ice thickness) and fresh water, both temporarily stored in form of sea ice, to be advected in accordance with proper sea-ice dynamics (i.e., including rheological properties). This is crucial for OGC models, where higher salinity occurs in areas of thermodynamic sea-ice growth (with subsequent deep convection). This sea ice is advected (presumably accompanied by ridging and rafting processes) and subsequently melted far remote from the location of its formation, inducing a freshening of the ocean surface layer (and thus a stable stratification). If such sea-ice related physical processes are not adequately considered in the coupling of atmosphere and ocean on GCM scales, unrealistic results are to be expected for long-time integrations. Finally, errors due to neglection of sea-ice physics in coupled GCM's are not restricted to the specific sea-ice regions and their boundary layers, but may extend over a global scale (Meehl and Washington, 1990), e.g., via an unrealistic simulation of the deep-water production.

Thus, the polar regions, where the ocean surface appears in a frozen stage, provide a unique environment for the verification of coupled atmosphere-ocean models, sea ice being the sensitive control variable for the skill of the simulations in terms of a proper exchange of heat, mass and momentum.

9. Acknowledgements

Thanks are due to P. Lemke, M. Heimann, K. Herterich, C. Koch, P. Loewe and E. Roeckner for valuable discussions and advice during this study, to L. Bengtsson, P. Lemke and K. Herterich for reviewing the manuscript, to W. D. Hibler, W. B. Owens, C. Koch and P. Lemke for providing their models, to M. Grunert for her laborious effort to finish the figures, to P. Besemann for updating the English language, to the Deutscher Wetterdienst (DWD), Offenbach, for delivering the global analyses of the ECMWF, and to R. Schnur for preprocessing these data. This work was supported by the Sonderforschungsbereich (SFB) 318.

REFERENCES

Andreas, E. L., Tucker, W. B. and Ackley, S. F. 1984. Atmospheric boundary-layer modification, drag coefficient, and surface heat flux in the Antarctic marginal ice zone. *J. Geophys. Res. 89*, 649–661.

Arya, S. P. S. 1975. A drag partition theory for determining the large-scale roughness parameter and wind stress on the Arctic pack ice. *J. Geophys. Res. 80*, 3447–3454.

Bengtsson, L. and Shukla, J. 1988. Integration of space and in situ observations to study global climate change. *Bull. Am. Met. Soc. 69*, 1130–1143.

Businger, J. A., Wyngaard, J. C., Izumi, Y. and Bradley, E. F. 1971. Flux profile relationships in the atmospheric surface layer. *J. Atmos. Sci. 28*, 181–189.

Cattle, H. and Roberts, D. L. 1988. The performance of atmospheric circulation models in polar regions. In: *Report of the 3rd session of the Working Group on Sea ice and climate WCRP-18*, TD-No. 272. Geneva/Switzerland: WMO, Annex A.

Claussen, M. 1991. Local advection processes in the surface layer of the marginal ice zone. *Boundary-layer Met. 54*, 1–27.

ECMWF Research Department 1985. Research manual 3, ECMWF forecast model, physical parameterisation. *Meteorological Bulletin M1.6/2(1)*. Reading/UK: ECMWF.

ECMWF Research Department 1986. Research manual 1, ECMWF data assimilation, scientific documentation. *Meteorological Bulletin M1.5/1(1)* (eds. P. Lönnberg and D. Shaw). Reading/UK: ECMWF.

Fiedler, F. and Panofsky, H. A. 1972. The geostrophic drag coefficient and the effective roughness length. *Q. J. R. Met. Soc. 98*, 213–220.

Foreman, S. J., Grahame, N. S., Maskell, K. and Roberts, D. L. 1988. Feedbacks and error mechanisms in a global coupled ocean/atmosphere/sea-ice model. In: *Modelling the sensitivity and variations of the ocean-atmosphere system WCRP-15, TD-No. 254.* Geneva/Switzerland: WMO, 271–279.

Gloersen, P. and Campbell, W. J. 1988. Variations in the Arctic, Antarctic and global sea ice covers during 1978–1987 as observed with the Nimbus 7 Scanning Multichannel Microwave Radiometer. *J. Geophys. Res. 93*, 10666–10674.

Gordon, A. L. and Huber, B. A. 1990. Southern Ocean winter mixed layer. *J. Geophys. Res. 95*, 11655–11672.

Hanssen-Bauer, I. and Gjessing, Y. T. 1988. Observations and model calculations of aerodynamic drag on sea ice in the Fram strait. *Tellus 40A*, 151–161.

Heimann, M. and Monfray, P. 1989. *Spatial and temporal variation of the gas exchange coefficient for CO_2: (1) data analysis and global validation.* Report No. 31. Hamburg/Germany: Max-Planck-Institut für Meteorologie.

Hibler, III, W. D. 1979. A dynamic thermodynamic sea ice model. *J. Phys. Oceanogr. 9*, 815–846.

Hibler, III, W. D. 1984. The role of sea ice dynamics in modeling CO_2 increases. *Geophys. Monogr. Am. Geophys. Un. 29*, 238–253.

Hibler, III, W. D. and Ackley, S. F. 1983. Numerical simulation of the Weddell Sea pack ice. *J. Geophys. Res. 88*, 2873–2887.

Hoeber, H. and Gube-Lehnhardt, M. 1987. The eastern Weddell Sea drifting buoy data set of the Winter Weddell Sea Project (WWSP). *Berichte zur Polarforschung 37.* Bremerhaven/Germany: Alfred-Wegener-Institut für Polar- und Meeresforschung.

Jacobs, S. S. and Comiso, J. C. 1989. Sea ice and oceanic processes on the Ross Sea continental shelf. *J. Geophys. Res. 94*, 18195–18211.

Janssen, P. A. E. M., Lionello, P., Reistad, M. and Hollingsworth, A. 1989. Hindcasts and data assimilation studies with the WAM model during the Seasat period. *J. Geophys. Res. 94*, 973–993.

Koch, C. 1988. A coupled sea ice-atmospheric boundary layer model, part I: description of the model and 1979 standard run. *Beitr. Phys. Atmos. 61*, 344–354.

Lemke, P. 1987. A coupled one-dimensional sea ice–ocean model. *J. Geophys. Res. 92*, 13164–13172.

Lemke, P., Owens, W. B. and Hibler, III, W. D. 1990. A coupled sea ice-mixed layer-pycnocline model for the Weddell Sea. *J. Geophys. Res. 95*, 9513–9525.

Leppäranta, M. 1981. On the structure and mechanics of pack ice in the Bothnian Bay. *Finn. Mar. Res. 248*, 3–86.

Louis, J. F. 1979. A parametric model of vertical eddy fluxes in the atmosphere. *Boundary-layer Met. 17*, 187–202.

Maier-Reimer, E., Mikolajewicz, U. and Hasselmann, K. 1991. *On the sensitivity of the global ocean circulation to changes in the surface heat flux forcing.* Report No. 68. Hamburg/Germany: Max-Planck-Institut für Meteorologie.

Manabe, S., Bryan, K. and Spelman, M. J. 1990. Transient response of a global ocean-atmosphere model to a doubling of atmospheric carbon dioxide. *J. Phys. Oceanogr. 20*, 722–749.

Martinson, D. G. 1990. Evolution of the Southern Ocean winter mixed layer and sea ice: open ocean deepwater formation and ventilation. *J. Geophys. Res. 95*, 11641–11654.

McPhee, M. G. 1980. An analysis of pack ice drift in summer. In: *Sea ice processes and models* (ed. R. S. Pritchard). Seattle/USA: University of Washington Press, 62–75.

Meehl, G. A. and Washington, W. M. 1990. CO_2 climate sensitivity and snow-sea ice albedo parameterisation in an atmospheric GCM coupled to a mixed-layer ocean model. *Clim. Change 6*, 283–306.

Mitchell, J. F. B. and Senior, C. A. 1989. The antarctic winter; simulations with climatological and reduced sea-ice extents. *Q. J. R. Met. Soc. 115*, 225–246.

Naval Polar Oceanography Center 1986. Antarctic ice charts 1985–1986. *Unclassified Antarctic ice charts.* Washington/USA: Navy/NOAA Joint Ice Center.

Oberhuber, J. M. 1990. *Simulation of the Atlantic circulation with a coupled sea ice-mixed layer-isopycnal general circulation model.* Report No. 59. Hamburg/Germany: Max-Planck-Institut für Meteorologie.

Overland, J. E. 1985. Atmospheric boundary layer structure and drag coefficient over sea ice. *J. Geophys. Res. 90*, 9029–9049.

Owens, W. B. and Lemke, P. 1990. Sensitivity studies with a sea ice-mixed layer-pycnocline model in the Weddell Sea. *J. Geophys. Res. 95*, 9527–9538.

Parkinson, C. L. and Washington, W. M. 1979. A large-scale numerical model of sea ice. *J. Geophys. Res. 84*, 311–337.

Schwerdtfeger, W. 1979. Meteorological aspects of the drift of ice from the Weddell Sea toward the mid-latitude westerlies. *J. Geophys. Res. 84*, 6321–6328.

Schwerdtfeger, W. 1984. Weather and Climate of the Antarctic. *Developments in Atmospheric Science 15.* Amsterdam/Holland: Elsevier Publ. Co.

Stössel, A. 1991. Application of an atmospheric boundary-layer model to a large-scale coupled sea-ice–oceanic mixed-layer model for the Southern Ocean. *Ann. Glaciol. 15*, 191–195.

Stössel, A., Lemke, P. and Owens, W. B. 1990. Coupled sea ice-mixed layer simulations for the Southern Ocean. *J. Geophys. Res. 95*, 9539–9555.

Trenberth, K. E. and Olson, J. G. 1988. ECMWF global analyses 1979–1986: circulation statistics and data evaluation. *Technical note TN-300 + STR.* Boulder/USA: NCAR.

Trenberth, K. E., Olson, J. G. and Large, W. G. 1989. A global ocean wind stress climatological based on ECMWF analyses. *Technical note TN-338 + STR.* Boulder/USA: NCAR.

van Ypersele, J.-P. 1986. *A numerical study of the response of the Southern Ocean and its sea ice to a CO_2-induced atmospheric warming.* Dissertation doctorale. Louvain-la-Neuve/Belgium: Université Catholique.

Wadhams, P., Lange, M. A. and Ackley, S. F. 1987. The ice thickness distribution across the Atlantic sector of the Antarctic Ocean in midwinter. *J. Geophys. Res. 92*, 14535–14552.

Worby, A. P. and Allison, I. 1991. Ocean-atmosphere energy exchange over thin, variable concentration Antarctic pack ice. *Ann. Glaciol. 15*, 184–190.